Journal of Engineering Mathematics (2006) 55: 255–276
DOI 10.1007/s10665-005-9018-x

Numerical investigation of non-stationary electrochemical shaping based on an analytical solution of the Hele-Shaw problem

V.P. ZHITNIKOV, G.I. FEDOROVA, N.M. SHERYKHALINA and A.R. URAKOV
Ufa State Aviation Technical University, 450000 Ufa, Russia (E-mail: zhitnik@ugatu.ac.ru)

Received 23 March 2004; accepted in revised form 29 August 2005 / Published online: 3 January 2006

Abstract. Transient processes occurring in electrochemical machining that lead to stationary, self-similar or other modes, are considered. These modes can apply to a part of the surface during a process for a limited time. The problem is formulated as a Hele-Shaw problem. Special high-precision numerical-analytical methods are developed for its solution The singularities of the solution are removed by representing it by the sum of a known function that includes the singularities and an unknown function without singularities. The unknown functions are determined by splines and a Schwarz integral.

Key words: electrochemical machining, self-similar solutions, transient process

1. Introduction

During electrochemical machining (ECM) the work piece (WP) is one of the electrodes, namely the anode, and the electrode-tool (ET) the cathode. The inter-electrode space (IES) is filled with an electrolyte. A current source connects the two electrodes and, as a result of this, dissolution takes place. By choosing the ET shape and its trajectory, we can obtain the required WP shape.

In the layers near the electrodes, which have very small widths, namely of the order of the size of molecules, the potential difference amounts to a few volts. During an ECM process the current heats the electrolyte. Apart from this, the current also causes electrolysis of the water. This means that hydrogen gas is produced on the cathode and oxygen gas on the anode. Moreover, the electrolyte will become polluted by reaction products. All these phenomena affect the electroconductivity of the electrolyte and also machining precision. The usual machining methods apply various techniques to improve machining precision. Pulse-cycle machining is used in particular, whereby the current is presented in the form of rectangular pulses. In the intervals between the pulses, the electrode tool is moved aside and a change of electrolyte takes place [1, Chapter 1], [2, Chapter 1], [3, Section 1.2].

Methods for solving the non-stationary problem usually involve a calculation of the current distribution and time shifts of surface points that are proportional to the current density. When the rate at which electrochemical dissolution takes place is low, we have the opportunity of using a quasi-stationary approach. Difficulties arise when local distances are considered that are comparable to the inverse of the local curvature. Under these conditions, numerical methods are not sufficiently accurate and complex approaches are required. Much work has been done in the field of non-stationary ECM by applying numerical methods to cases where the inter-electrode channel has a low curvature. This is so-called one-dimensional electrochemical shaping. Extensive reviews of such investigations can be found in [4, Section 1.2],

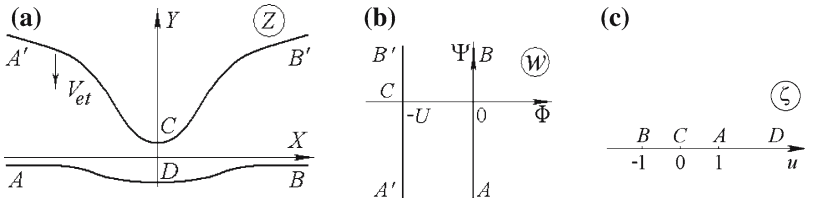

Figure 1. Domain shapes on different planes (a) The interelectrode space (b) Complex potential plane (c) Parametric ζ plane.

[5, Chapter 2], [6]. Numerical modelling of two-dimensional non-stationary ECM for different machining set-ups involves finite-difference and finite-element methods [7, 8] and boundary-element methods [9–11]. Three-dimensional cases were considered in [12].

2. Reduction to a Hele-Shaw problem

As an example let us consider the two-dimensional ECM problem, when an electrode-tool $A'CB'$ moves vertically downwards with velocity V_{et} (Figure 1a). The dissolving surface of the work piece is ADB.

The electrochemical dissolution process is described by Faraday's law

$$\mathrm{d}\,m = \frac{M}{nF} J \eta \,\mathrm{d}t, \quad m = \rho A h, \tag{1}$$

where m is the mass of the dissolved material, M, n are the atomic mass and valency of the WP material, $F = N_{\mathrm{A}} e$ is the Faraday number, N_{A} is the Avogadro number, e is the electron charge, t is the time, η is the current efficiency (fraction of current, used for the main process of metal dissolution), ρ is the WP metal density, $J = Aj$ is the current, j is the current density, A is the WP area, h is the dissolved metal thickness. The current efficiency may depend on the current density or can be a constant (depending on the process conditions and problem statement). According to Ohm's law, $j = \kappa E$, where κ is the electrolyte conductivity and E is the electric-field-strength vector. Applying expression (1) to a small area of the WP surface, we obtain

$$\frac{\mathrm{d}\,h}{\mathrm{d}\,t} = k \eta E_{\mathrm{n}}, \quad k = \frac{M \kappa}{nF\rho}. \tag{2}$$

If we consider equipotential surfaces, then the streamlines are perpendicular to the work piece. In another case the normal part E_{n} of the electric-field-strength vector is effective for the ECM process.

We consider an ideal model of the machining process, when the anode and cathode potentials do not depend on time, gassing and electrolyte heating are not essential, and thus we can assume the electroconductivity to be constant in time and space. In this case the vector field of the electric strength is potential and solenoidal. Thus, for the problem solution we can use complex-variable methods. For each time the solution is sought as an analytic function of the complex variable $W(Z)$, where $Z = X + \mathrm{i}Y$, X, Y are the Cartesian coordinates of the IES points, $W = \Phi + \mathrm{i}\Psi$ is the complex potential, Φ is the electric field potential, Ψ is the stream function. The electric field strength is given by $E = \overline{\dfrac{\mathrm{d}W}{\mathrm{d}Z}}$.

If equipotential electrodes are considered, (the potential of the work piece ADB equals 0, the potential of ET equals $-U$), the complex potential domain, corresponding to IES is a vertical strip (Figure 1b) and does not depend on time. In other cases the domain may have another form (for example, a curvilinear strip) and can depend on time.

This problem with condition (2) is equivalent to the well-known Hele-Shaw free-boundary problem [13–17]. It is important to notice that this boundary condition is sufficient to construct numerical methods for ECM problems without any additional analytical transformations. Methods involving finite or boundary elements are traditionally used for solving ECM problems. These methods are very convenient to obtain solutions for IES of different shapes [8–12]. But a simplicity of methodology is usually accompanied by a lower order of precision. It does not cause an essential error, if the relative distance change during the process is not large. In this case such methods may well satisfy practical requirements. If the process is of long duration, then an accumulation of essential errors may arise. These errors can hardly be compensated by increasing the number of nodes because of the nonlinear rate of calculations growth. This leads to the necessity of constructing new advanced methods to solve numerically the unsteady ECM problem.

Below, both the WP and the ET shapes will be described by a parametric complex function $Z(u,t)$, where u is a real variable. The particular value of this variable determines the position of a surface point. In order to solve this problem with the help of complex-variable function theory, the IES is conformally mapped onto a domain ζ of simple geometric shape (for example, an upper half plane), upon which the parameter u can be taken equal to a value ζ on the real axis. In contrast to the physical plane, the shape of the domain in the parametric-variable plane is the same at any time with three points being fixed. So, the problem can be reformulated in parametric form: to find two analytic functions $Z(\zeta,t), W(\zeta)$ (or $W(\zeta,t)$ in the general case). To calculate the solution at a next time instant, the derivative $\frac{\partial Z}{\partial t}(\zeta,t)$ has to be calculated by using condition (2).

Suppose the angle of the tangent to the WP surface with the X-axis is θ. Then the normal displacement of the surface $\mathrm{d}h$ and the normal strength E_n are given as $\mathrm{d}h = \Im\mathfrak{m}\left(\mathrm{e}^{-\mathrm{i}\theta}\mathrm{d}Z\right)$, $E_\mathrm{n} = \Im\mathfrak{m}\left(\mathrm{e}^{-\mathrm{i}\theta}E\right)$. Since $\frac{\partial Z}{\partial u} = \pm\left|\frac{\partial Z}{\partial u}\right|\mathrm{e}^{\mathrm{i}\theta}$, Equation (2) is equivalent to the equality

$$\Im\mathfrak{m}\left(\overline{\frac{\partial Z}{\partial u}}\frac{\mathrm{d}Z}{\mathrm{d}t}\right) = \Im\mathfrak{m}\left(\overline{\frac{\partial Z}{\partial u}}\frac{\partial Z}{\partial t} + \overline{\frac{\partial Z}{\partial u}}\frac{\partial Z}{\partial u}\frac{\mathrm{d}u}{\mathrm{d}t}\right) = \Im\mathfrak{m}\left(\overline{\frac{\partial Z}{\partial u}}\frac{\partial Z}{\partial t}\right) = k\eta\,\Im\mathfrak{m}\left(E\overline{\frac{\partial Z}{\partial u}}\right). \tag{3}$$

Here a bar denotes the complex conjugate. The electric field strength at the boundaries is equal to

$$E = \overline{\frac{\partial W}{\partial u}}\left(\overline{\frac{\partial Z}{\partial u}}\right)^{-1}. \tag{4}$$

Then, considering (4), we have that condition (3) can be written as

$$\Im\mathfrak{m}\left(\frac{\partial Z}{\partial t}\overline{\frac{\partial Z}{\partial u}}\right) = -k\eta\frac{\partial \Psi}{\partial u}. \tag{5}$$

The boundary condition (5) is treated as an equation with respect to $\frac{\partial Z}{\partial t}(\zeta,t)$ on the boundary of the IES. Once the equation has been solved, this derivative in the IES is reconstructed as a solution of the boundary-value problem for the analytical function $\frac{\partial Z}{\partial t}(\zeta,t)$.

On the boundary parts corresponding to the electrode tool surface, dissolution does not occur, so the right part of Equation (5) on this boundary is zero (in a coordinate system connected to ET). Therefore, the unknown derivative $\frac{\partial Z}{\partial t}(\zeta,t)$ can be obtained as the solution of a Riemann-Hilbert boundary-value problem.

Equation (5) is equivalent to the Polubarinova-Galin equation [15, 17–20] for the Hele-Shaw problem. As in [17, Equation (1.17)] its solution can be obtained by using Schwarz's

integral. We shall do this later after singularities have been removed for numerical convenience.

3. Calculation of surface shapes that are independent of time

For comparison with further non-stationary numerical solutions and the testing of algorithms, let us consider first some special cases of solutions of (5).

3.1. Stationary electrochemical shaping

In many ECM processes the most interesting aspect is the shaping stage, when the IES geometry shape is time-invariant in spite of the ET moving into the WP body. During the shaping stage, in the fixed coordinate system (X, Y), the surface is moving together with the ET at a velocity V_{et}. In the moving-coordinate system, $Z = Z_1 + V_{et}t$, Equation (5) takes the form

$$\Im\mathrm{m}\left[V_{et}\overline{\frac{\partial Z_1}{\partial u}}\right] = -k\eta\frac{\partial\Psi}{\partial u}, \quad \text{or} \quad \Im\mathrm{m}\left[V_{et}\overline{\frac{\partial Z_1}{\partial\Psi}}\right] = -k\eta.$$

For example, if V_{et} is directed along the Y-axis ($V_{et} = -\mathrm{i}|V_{et}|$) and the work piece is equipotential (then $W = \mathrm{i}\Psi$ on WP surface), the boundary condition takes the form

$$\Im\mathrm{m}\frac{\mathrm{d}Z_1}{\mathrm{d}W} = -\frac{k\eta}{|V_{et}|}. \tag{6}$$

If $\eta = \text{const}$, this equation represents the arc of a circle with radius $R = \frac{1}{2}\frac{|V_{et}|}{k\eta}$ and centre at the point $0 + \mathrm{i}R$ on the strength hodograph plane $\mathrm{d}W/\mathrm{d}Z_1$ [4]. Thus, this condition is analogous to the condition on the free surface of a steady flow of a viscous fluid subjected to gravity [20].

We introduce the dimensionless variables $w = \varphi + \mathrm{i}\psi = W/U$, $z = x + \mathrm{i}y = |V_{et}|\,Z/k\eta U$. Then (6) can be written as follows

$$\Im\mathrm{m}\frac{\mathrm{d}z_1}{\mathrm{d}w} = -1. \tag{7}$$

Let us consider a stationary problem which has a simple analytic solution. The boundary configuration must be analogous to IES, as demonstrated in Figure 1a. The solution is sought as the sum $z_1(\zeta) = z_0(\zeta) + z_\Delta(\zeta)$. The function $z_0(\zeta)$ is assumed to be the function mapping the upper half plane ζ (Figure 1c) onto a horizontal strip of unit width:

$$z_0(\zeta) = -\mathrm{i}w = \frac{1}{\pi}\log\frac{\zeta - 1}{\zeta + 1}. \tag{8}$$

Then $\Im\mathrm{m}\frac{\partial z_0}{\partial w} = -1$, whence according to (7), $\Im\mathrm{m}\frac{\partial z_\Delta}{\partial w} = \mathrm{Re}\frac{\partial z_\Delta}{\partial u} = 0$.

As the shape of domain z_Δ, a circle of radius α with the a from 0 to $\mathrm{i}\tilde{\gamma} = \mathrm{i}(1+\gamma)\alpha$, $-1 < \gamma < 1$, is chosen (see Figure 2a).

The upper half plane ζ is mapped onto the plane z_Δ domain by the following function

$$z_\Delta(\zeta) = -2\mathrm{i}\alpha\frac{(\gamma+1)^2\left(\zeta^2-1\right) - \left(1-\gamma^2\right)\zeta\sqrt{\zeta^2-1}}{(\gamma+1)^2 - 4\gamma\zeta^2}. \tag{9}$$

Results of calculations for different values of the parameter γ are presented in Figure 2b, where the upper curves correspond to the ET surface shapes and the lower curves to the WP shapes.

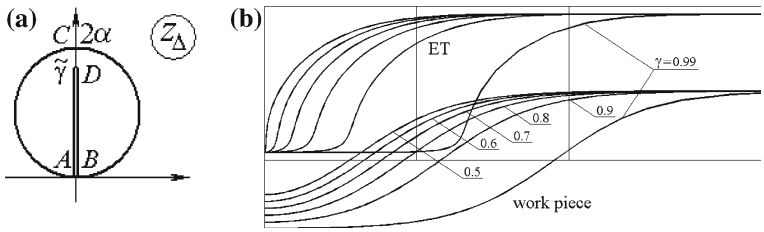

Figure 2. Stationary ECM: (a) the z_Δ domain; (b) IES shapes for $\alpha = 0{\cdot}9$.

3.2. Self-similar solutions

3.2.1. *The self-similar boundary condition*

The self-similar property is borne out by the preservation of geometrical homothetic of the interelectrode space with respect to a fixed point Z_C. If some typical size $l(t)$ is chosen as the scale factor, then

$$z(\zeta) = \frac{Z(\zeta, t) - Z_C}{l(t)}$$

is a dimensionless analytic function that is independent of time. As the shape of IES in the parametrical variable plane does not change, the partial derivative reads

$$\frac{\partial Z}{\partial t} = \alpha(t)\, l(t)\, z(\zeta), \quad \alpha(t) = \frac{1}{l(t)} \frac{\mathrm{d}l}{\mathrm{d}t}, \tag{10}$$

where $\alpha(t)$ is the relative speed of the scale-factor change. Considering (10) and presenting the complex potential as $W = U w = U(\varphi + \mathrm{i}\psi)$, where U is a scale factor, we obtain from equality (5)

$$\Im\mathrm{m}\left(z \frac{\overline{\partial z}}{\partial \psi}\right) = -\frac{1}{\lambda}, \quad \lambda = \frac{l^2 \alpha}{k \eta U}. \tag{11}$$

After substitution of $z = \mathrm{e}^{\chi}$, where $\chi = \mu + \mathrm{i}\nu = \log z$, in (11), we get

$$\mathrm{e}^{2\mu} \frac{\partial \nu}{\partial \psi} = \frac{1}{\lambda}. \tag{12}$$

This is the boundary condition of the self-similar problem.

The value of the component of the strength vector normal to a boundary can be obtained from

$$\left|\frac{\partial \Re\mathrm{e}\, w}{\partial n}\right| = \left|\frac{\partial z}{\partial \psi}\right|^{-1} = \lambda \mathrm{e}^{\mu} \left[\left(\frac{\mathrm{d}\mu}{\mathrm{d}\nu}\right)^2 + 1\right]^{-1/2}.$$

The value of the non-dimensional constant λ in (12) should be determined as a part of the solution.

If U and η are constant, then λ is independent of time if and only if $l\mathrm{d}l/\mathrm{d}t$ is constant. The latter condition provides

$$\alpha(t) = \left(2t + \alpha^{-1}(0)\right)^{-1}, \quad l(t) = l(0)\sqrt{1 + 2\alpha(0)\, t}. \tag{13}$$

Hence we can consider $t = -\frac{1}{2\alpha(0)} = -\frac{l^2(0)}{2k\eta U\lambda}$ as the time when the dissolution process of some initial singular work-piece shape begins. Taking into account the fact, that a self-similar process is an attractor to which a nonstationary process apparently converges, gives the opportunity to avoid difficulties in starting calculating the dissolution of surfaces, having initially a cusped shape or conductor-isolator contact.

3.2.2. *Reduction to a hydrodynamic problem*

There are several solutions of (11) obtained by Polubarinova-Kochina methods and their modifications [18–22]. Here we use another method. It is based on reducing the original problem to the well-known hydrodynamical problem of the flow about a circular arc [23–25].

Let us consider problems with equipotential boundaries and constant current efficiency η. Notice that condition (12) is similar to the boundary condition in the problem of external flow over a circular arc of radius R by a stream of ideal liquid

$$-\frac{1}{R} = \frac{\mathrm{d}\theta}{\mathrm{d}s} = V_0 \mathrm{e}^{\tau_f} \frac{\mathrm{d}\theta}{\mathrm{d}\Phi_1} \tag{14}$$

formulated with the help of the analytic Levi-Chivita function $\omega = \log \frac{1}{V_0} \frac{\mathrm{d}W_1}{\mathrm{d}Z_1} = \tau_f - \mathrm{i}\theta$, where $Z_1 = X_1 + \mathrm{i}Y_1$ defines the flow-plane point coordinates; $W_1 = \Phi_1 + \mathrm{i}\Psi_1$ is the complex potential of the flow, s is the arc abscissa, V_0 is a typical velocity, θ denotes the angle of inclination with respect to the X_1-axis of the fluid velocity vector. To consider this auxiliary hydrodynamical problem, let us represent (14) in dimensionless form

$$-\frac{a_0}{R} = \mathrm{e}^{\tau_f} \frac{\mathrm{d}\theta}{\mathrm{d}\varphi_1}, \tag{15}$$

where a_0 is a typical linear size, $\Phi_1 = a_0 V_0 \varphi_1$, $W_1 = a_0 V_0 w_1$, $z_1 = Z_1 / R$.

To turn this equation into the same form as (12), let us assume $\omega = 2\chi$ (in this case $\tau_f = 2\mu, \theta = -2\nu$). Besides we state the relation between the electrical and hydrodynamical complex potential planes. While the equipotential boundaries have to correspond to the impenetrable ones, we state $w_1 = -\mathrm{i}w$ (so, $\varphi_1 = \psi$). It is seen that under this condition

$$\lambda = \frac{l^2\alpha}{k\eta U} = 2\frac{R}{a_0} \tag{16}$$

and Equation (12) coincides with (15).

Therefore, the solution of the electrochemical problem is given by

$$z = \mathrm{e}^{\omega/2} = \sqrt{\frac{a_0}{R}\frac{\mathrm{d}w_1}{\mathrm{d}z_1}}, \tag{17}$$

where $w_1(z_1)$ is the solution of the hydrodynamic problem.

When taking the logarithm of z, we have to draw a cut from the point $z = 0$ to infinity (if the point $z = 0$ is not on the boundary), then the domain corresponding to IES in the z_1-plane can be a circular triangle or a more complex figure. Thus, first, the hydrodynamic analogy allows reducing the problem to that of conformal mapping (which, according to Riemann theorem, solves the problem about existence and uniqueness of the solution). Second, it gives us the possibility to obtain an analytical solution for some cases. Third, in more complicated cases, it allows us to apply the numerical methods developed earlier for hydrodynamical problems to solve the electrochemical problem.

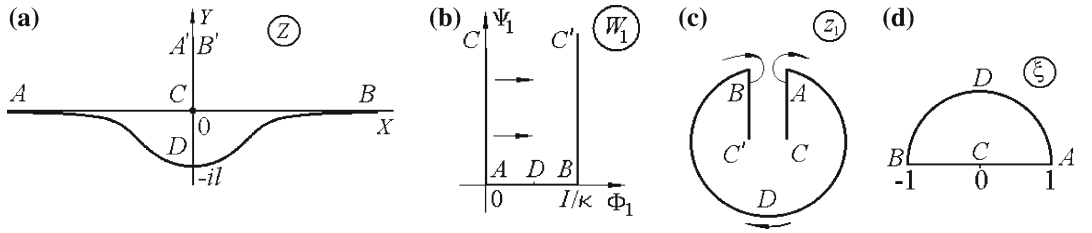

Figure 3. The self-similar ECM for a wire ET: (a) physical plane, (b) complex potential plane of the auxiliary flow, (c) physical plane of the auxiliary flow, (d) plane of the parametric variable.

3.2.3. *The problem of self-similar processing for a wire-shaped electrode-tool*

Let us consider the problem of non-stationary self-similar processing with a wire ET. In the cross-section the ET is represented by a point C (Figure 3a). Let us place the origin of the coordinate system at the centre of similarity; this is at the point C. The domain which corresponds to IES in the plane of the complex potential W is a half-strip of width I/κ, where I is the "plane" electric current $I = J/b$ (current flowing through an electrochemical unit of width $b = 1$). The horizontal boundaries of the half-strip correspond to the edges of the cut $A'CB'$ in the Z-plane, drawn vertically upwards from the point C. The complex potential $W_1 = w_1 I/\kappa = -\mathrm{i}W$ in the domain of the auxiliary flow is shown in Figure 3b, where arrows show the images of the streamlines.

Let us construct the auxiliary flow in the plane z_1 (Figure 3c). As was mentioned above, the surface of the work piece corresponds to a circular arc in the plane z_1. According to the rule of conformity $\theta = -2\nu$ (ν is the argument of Z, but θ is an angle of inclination of the fluid velocity vector). So, at the point A ($\nu = -\pi$) we have $\theta = 2\pi$, at point B ($\nu = 0$): $\theta = 0$. Thus, the image of the treated self-similar surface is a complete circle ADB in the z_1-plane.

On the cut CB' we have $\nu = \pi/2$; then $\theta = -\pi$. Taking into account that fluid flows out of the domain through BC' (see streamline images in Figure 3b) in a direction normal to the boundary, we find that BC' is a ray, directed downwards to the z_1-plane. Since at another cut CA' we have $\nu = -3\pi/2, \theta = 3\pi$, CA' in the z_1-plane corresponds to the ray AC, directed as BC'. The fluid flows into the domain through AC.

The flow domain constructed (Figure 3c) thus consists of two sheets and the lines BC' and AC' have identical Cartesian coordinates.

Conformal mapping of IES from plane z_1 to the plane w_1 is made by use of the parametrical plane ξ (upper half disk, see Figure 3d)

$$w_1 = -\frac{\mathrm{i}}{\pi}\log\xi, \quad z_1 = \mathrm{i} + \frac{\mathrm{i}(\xi^2-1)^3}{\xi^4(3-\xi^2)}.$$

Then the complex potential $w = W\kappa/I$ of the ECM problem is equal to $w = (\log\xi)/\pi$. With the help of (17) we find the conformal mapping of the parametrical plane ξ onto the plane z

$$z = -\mathrm{i}\sqrt{\frac{a_0}{R}}\frac{\xi^2(3-\xi^2)}{\sqrt{12\pi}(\xi^2-1)}.$$

According to Figures 3a and 3d, $z(\mathrm{i}) = -\mathrm{i}$. Hence $a_0/R = 3\pi$. Therefore, using (16) with $U = I/\kappa$, we can define the dimensionless constant $\lambda = 2/(3\pi)$. Finally we obtain

$$z = -\mathrm{i}\frac{\xi^2(3-\xi^2)}{2(\xi^2-1)}. \tag{18}$$

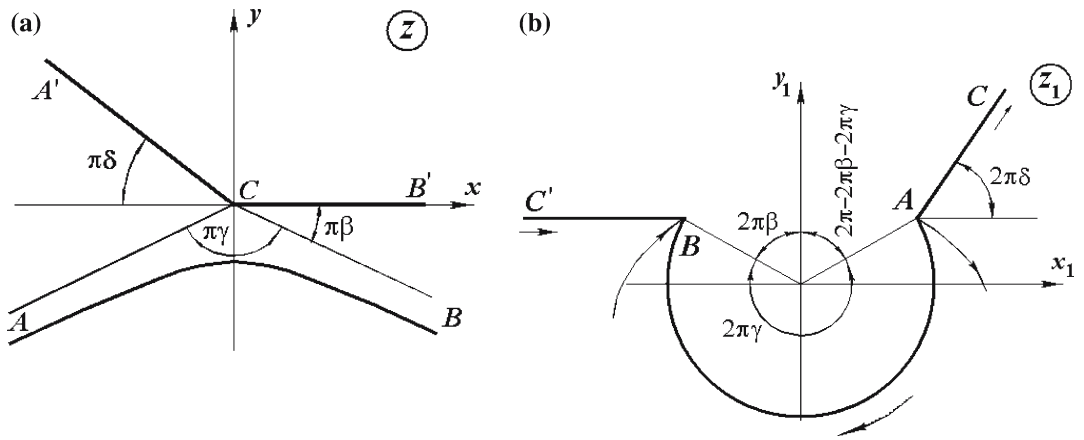

Figure 4. Self-similar electrochemical machining by a wedge-shaped ET: (a) physical plane, (b) the plane of auxiliary flow.

3.2.4. *The problem of a wedge-shaped electrode-tool*

The method described above is now used for the solution of the problem of a wedge-shaped ET machining a surface inscribed in the angle $\pi\gamma$ (Figure 4a). On the complex potential plane w, the $\varphi = 0$ axis corresponds to the WP boundary (the potential of this surface is assumed to be zero). As the potential of the cathode is negative, let us consider a strip corresponding to the IES domain in the complex potential plane (Figure 1b).

Let us consider the auxiliary flow formed in the plane z_1 which corresponds to the vector field of the electric intensity under a self-similar ECM. The circular arc corresponds to the WP surface and the external flow over the arc corresponds to the IES. Moving along the WP surface from B to A, we note that the argument of the anode surface point changes from $-\beta\pi$ to $-\gamma\pi - \beta\pi$ (Figure 4a). Correspondingly, θ changes from $2\beta\pi$ to $2\beta\pi + 2\gamma\pi$ (see Figure 4b).

The plane w_1 can be obtained by rotating the plane w clockwise through 90°. We note that the horizontal strip on the w_1-plane corresponds to the stream of fluid flowing from point source A to point sink B. The source and the sink are placed on the circular arc.

The argument of any point of the ET surface CB' on the z-plane is equal to zero; hence $\theta = 0$. The argument of points on the ET surface $A'C$ is $-\pi - \delta\pi$, hence $\theta = 2\pi + 2\delta\pi$. The boundaries AC and BC' on the z_1-plane are the streamlines, and thus these boundaries are the rays directed according to the mentioned angles.

The boundary-angle jump at point B is equal to $2\beta\pi$ (Figure 4b); at point A it is equal to $2\pi(1 - \beta - \gamma + \delta)$. The third angle in the point C, placed at infinity, is equal to $-(\pi + 2\delta\pi)$.

The solution of the hydrodynamical problem is now reduced to a conformal mapping of the upper half-plane ζ, where the images of the singular points A, B, C are $\zeta = 0, 1, \infty$, respectively, onto the flow domain z_1 which is a triangle with circular edges. This is realised by standard means with the help of hypergeometric functions ${}_2F_1(a, b, c, \zeta)$, *i.e.*, a linear-fractional combination of two linearly independent integrals of a Gauss differential equation.

For this problem we have $w_1(\zeta) = -\frac{1}{\pi}\log\frac{\zeta - 1}{\zeta}$. Choosing any point ζ_0, where, for example, $|z(\zeta_0)| = 1$, (say, point D), we have from (17) $\frac{a_0}{R}\left|\frac{\mathrm{d}w_1}{\mathrm{d}z_1}(\zeta_0)\right| = 1$. After $z_1(\zeta)$ has been determined, we find

$$\frac{a_0}{R} = \left|\pi\zeta_0(1 - \zeta_0)\frac{\mathrm{d}z_1}{\mathrm{d}\zeta}(\zeta_0)\right|.$$

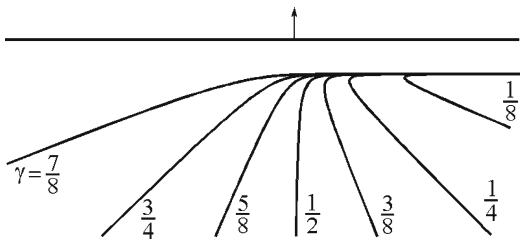

Figure 5. Shapes of self-similar surface for $\delta=0, \beta=0, (\lambda=1)$.

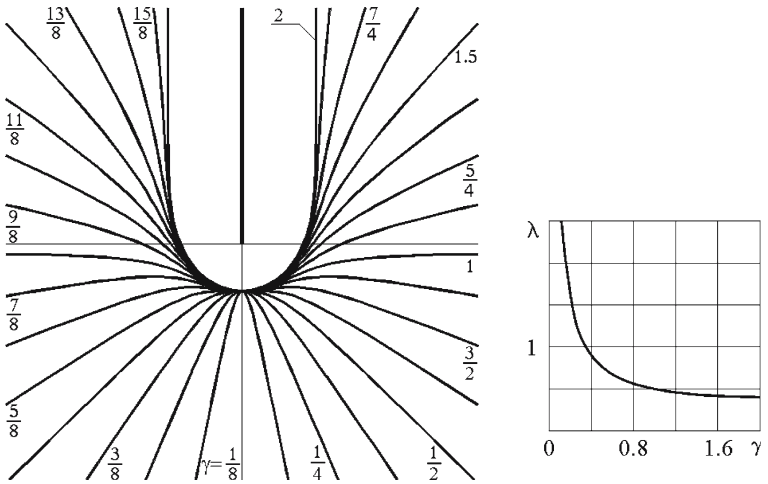

Figure 6. Shapes of self-similar surface for $\delta=1,\ 2\beta=\delta-\gamma+1$ (rotated trough 90° contraclockwise).

The ratio $\lambda=2R/a_0$ is the dimensionless constant (16), which determines the rate of dissolution. The solution of the electrochemical problem is given by (17).

Figures 5 and 6 show the forms of the self-similar surfaces as predicted by the solutions of the electrochemical problem and the corresponding values of the constant λ depending on the angle coefficient γ. The values of the angle coefficient γ are given in the figures.

For many special cases the obtained solution can be represented in simpler form without the use of hypergeometric functions. This is so when all sides of the circular triangle (or its extensions) have a single intersection point. In another case straight sides (or their extensions) have an intersection at the center of the circle. For example the solutions for $\beta=0, \gamma=1$ (ADB is a complete circle) are presented in Table 1. For all these solutions we have $\lambda=1$.

This problem has been solved before [21, 22] for the symmetrical case $\beta=0, \gamma=1+\delta$ (the asymptotes of the free surface are parallel to the wedge sides). In Figure 6 a solution of this kind is depicted by a curve with $\gamma=2$. The asymmetric case and cases for which $\beta\neq0, \gamma\neq 1+\delta$ have not been studied so far.

3.2.5. *The problem of a wedge-shaped electrode tool with two isolated sides*

The difference between this problem and that studied in the previous section is the role of the rays AC and BC' in the z_1-plane. They are equipotential flow boundaries now, so they are normal to streamlines. While $\theta=0$ on BC', this ray is directed vertically upwards for $\beta=0$ or downwards for $\beta\geq 1/4$. Let us consider the second case.

The auxiliary complex potential-flow domain is the upper half plane with a cut from $w_1=$ i(C) to i∞ (A', B'); the points A and B are dipoles. Then $w_1(\zeta)=\frac{i}{2}\frac{2\zeta-1}{\sqrt{\zeta(\zeta-1)}}$. So, the angles

Table 1. Analytic solutions of the problem for $\beta = 0, \gamma = 1$.

δ	$z(\zeta)$
0	$-\frac{1}{\pi}\log\frac{\zeta-1}{\zeta}$
0·25	$-\frac{\sqrt[4]{\zeta}}{\pi}\left(\log\frac{\sqrt{\zeta}-1}{\sqrt{\zeta}+1}+\frac{2}{\sqrt{\zeta}}\right)$
0·5	$-\frac{\sqrt{\zeta}}{\pi}\left(\log\frac{\zeta-1}{\zeta}+\frac{1}{\zeta}\right)$
0·75	$-\frac{\zeta^{3/4}}{\pi}\left(\log\frac{\sqrt{\zeta}-1}{\sqrt{\zeta}+1}+\frac{2}{3\zeta\sqrt{\zeta}}+\frac{2}{\sqrt{\zeta}}\right)$
1	$-\frac{\zeta}{\pi}\left(\log\frac{\zeta-1}{\zeta}+\frac{1}{2\zeta^2}+\frac{1}{\zeta}\right)$

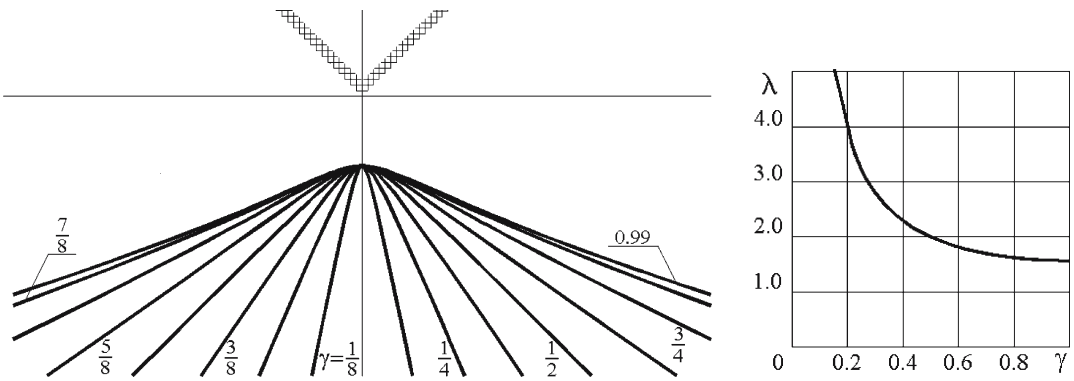

Figure 7. Shapes of self-similar surface for $\delta = 0{\cdot}5, 2\beta = \delta - \gamma + 1$ (rotated through 45° contraclockwise).

of the circular triangle are:

$$A : \pi\left(\frac{3}{2} + 2\delta - 2\beta - 2\gamma\right), \quad B : 2\beta\pi - \frac{\pi}{2}, \quad C : -2\delta\pi.$$

Solutions, for which the asymptotes of the WP surface are in a symmetrical position relative to the bisectrix of the wedge, are illustrated in Figure 7. Here the dependence $\lambda(\delta)$ for this case is also presented. Solutions for $\delta = 1$ were considered in [24].

4. Solution of non-stationary ECM problems

The usual method has a following numerical solution scheme:

(1) for t=0 the primary anode shape $Z(\zeta, 0)$ is fixed;
(2) the electric-field strength in selected WP points is determined;
(3) a time step is executed, and as part of this process, according Faraday's law, a shift of every point perpendicular to the surface, proportional to the field strength $\mathrm{d}Z = k\eta E_{\mathrm{n}}\mathrm{d}t$, takes place;
(4) the surface shape is calculated by using the new positions of these points, upon which we return to step 2.

Solving the problem numerically following this scheme, we can incur an uncontrolled increase of the distances between the nodes. This process leads to divergence of the numerical solution [12]. When non-stationary problems are solved, Equation (5) allows us to move the surface points along the vector $\partial Z/\partial t$ and to find the surface position at the next time instant. We suggest fixing the nodes on the boundary of a variable parametric plane. This makes it possible to control the variations of the solution in time and avoid large variations. This modification can stabilise non-stationary methods of solution [26, 27].

Let us consider a non-stationary electrochemical problem with the inter-electrode space section as presented in Figure 1a, assuming that the ET boundary has a horizontal asymptote. The developed method allows us to consider the variable η and electrode potentials, for instance as functions of the kind $\eta(\kappa E), \varphi_a(\kappa E), \varphi_c(\kappa E)$. However, the actual functions essentially depend on the electrode material, electrolyte consistency and other physical parameters. Thus, studying the process with prescribed functions gives little information. Studying all the process functions simultaneously is very complex and must be preceded by basic investigations of the process independent of these factors. So, in this paper the current efficiency η and the electrode potentials are considered to be constant. Then the domain of the complex potential W is a vertical strip (Figure 1b).

It is more convenient for us to use dimensionless values in our calculations. In particular, the complex potential is expressed as $W = Uw = U(\varphi + i\psi)$. Dimensionless coordinates and time are introduced as follows

$$z = Z/l, \quad x = X/l, \quad y = Y/l, \quad \tau = k\eta U t/l^2, \tag{19}$$

where l is a typical size independent of time. For an ET moving at a velocity V_{et} the l value is assumed to be equal to the stationary gap for a plane-parallel IES $l = k\eta U/|V_{et}|$. Then the modulus of the dimensionless ET speed is equal to 1. The non-dimensional time is equal to the non-dimensional ET shift.

4.1. Method of solution for the non-stationary problem

The inter-electrode space and the complex potential plane are conformally mapped onto a strip $\chi = \sigma + i\upsilon$ (Figure 8). A strip is a more convenient domain for our numerical methods, because all functions obtained feature rapidly decreasing exponents at infinity and can be approximated without essential error. Using another domain, for instance a half-plane or a disk, we may have to deal with functions that have singularities with infinite derivatives.

The image of the inter-electrode space in the w-plane is a vertical strip. Then

$$w(\chi) = i\chi, \quad \frac{\partial\psi}{\partial\sigma} = 1. \tag{20}$$

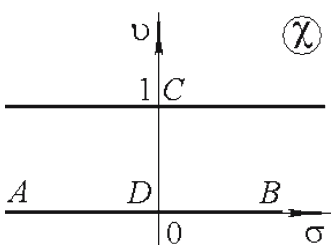

Figure 8. The auxiliary χ plane.

As we can see from the problem statement, the function $z(\chi,\tau)$ tends to infinity for $\sigma\to\pm\infty$. This implies that the Schwarz formula cannot be used. We suggest decomposing the function $z(\chi,\tau)$ as follows:

$$z(\chi,\tau)=g(\tau)z_0(\chi)+c\tau+z_\Delta(\chi,\tau),$$

where the imaginary part $\Im\mathrm{m}\, z_\Delta(\sigma+\mathrm{i}\upsilon,\tau)\to 0$ when $\sigma\to\pm\infty$, so that the function $z_\Delta(\chi,\tau)=x_\Delta+\mathrm{i}y_\Delta$ is continuous on the boundary. Let us choose $z_0(\chi)=\chi$. Using the obvious plane-parallel IES relations, we define

$$g(\tau)=y_{B'}(\tau)-y_B(\tau),\quad c=-\frac{\mathrm{i}}{g(\tau)},\quad \frac{\mathrm{d}g}{\mathrm{d}\tau}(\tau)=\frac{1}{g(\tau)}-1.$$

In dimensionless variables the boundary condition (5) takes the form

$$\Im\mathrm{m}\left(\frac{\partial z_\Delta}{\partial\tau}\overline{\frac{\partial z}{\partial\sigma}}\right)=\frac{\partial y_\Delta}{\partial\sigma}\frac{\mathrm{d}g}{\mathrm{d}\tau}\sigma+\frac{1}{g}\frac{\partial x_\Delta}{\partial\sigma},\quad \chi=\sigma, \tag{21}$$

$$\Im\mathrm{m}\left(\frac{\partial z_\Delta}{\partial\tau}\overline{\frac{\partial z}{\partial\sigma}}\right)=\frac{\partial y_\Delta}{\partial\sigma}\frac{\mathrm{d}g}{\mathrm{d}\tau}\sigma,\quad \chi=\sigma+\mathrm{i}. \tag{22}$$

Let us present the unknown derivative as a product of analytical functions $\frac{\partial z_\Delta}{\partial\tau}(\chi,\tau)=\mathrm{i}\frac{\mathrm{d}z}{\mathrm{d}w}(\chi,\tau)\,f(\chi,\tau)$ and substitute the product in (21) and (22). On the equipotential boundary $w=\mathrm{i}\psi$ we have

$$\Im\mathrm{m}\left(\mathrm{i}\overline{\frac{\partial z}{\partial\sigma}}\frac{\mathrm{d}z}{\mathrm{d}w}f\right)=\Im\mathrm{m}\left(\overline{\frac{\partial z}{\partial\sigma}}\frac{\partial z}{\partial\sigma}\left(\frac{\partial\psi}{\partial\sigma}\right)^{-1}f\right)=\left|\frac{\mathrm{d}w}{\mathrm{d}z}\right|^{-2}\Im\mathrm{m}\, f.$$

With regard to (20), the equalities (21), (22) take the form

$$\Im\mathrm{m}\, f=\left|\frac{\mathrm{d}w}{\mathrm{d}z}\right|^2\left(\frac{\partial y_\Delta}{\partial\sigma}\frac{\partial g}{\partial\tau}x_0+\frac{1}{g}\frac{\partial x_\Delta}{\partial\sigma}\right),\quad \chi=\sigma, \tag{23}$$

$$\Im\mathrm{m}\, f=\left|\frac{\mathrm{d}w}{\mathrm{d}z}\right|^2\frac{\partial y_\Delta}{\partial\sigma}\frac{\partial g}{\partial\tau}x_0,\quad \chi=\sigma+\mathrm{i}. \tag{24}$$

The analytical function $f(\chi,\tau)$ can now be found with the Schwarz formula.

4.2. Solution algorithm

Firstly, it is necessary to find a conformal mapping of χ onto the initial inter-electrode domain $z(\zeta,0)$. The solution is found in the σ_m nodes. On each time step $\tau_j=j\Delta_\tau$ the decision parameters are $y_m=\Im\mathrm{m}\, z_\Delta(\sigma_m,\tau_j)$ and $y'_m=\Im\mathrm{m}\, z_\Delta(\sigma'_m+\mathrm{i},\tau_j)$. The values of $y_\Delta(\sigma,\tau_j)=\Im\mathrm{m}\, z_\Delta(\sigma,\tau_j)$ and $y_\Delta(\sigma+\mathrm{i},\tau_j)=\Im\mathrm{m}\, z_\Delta(\sigma+\mathrm{i},\tau_j)$ at the internal points between the nodes are determined by means of cubic splines, with two continuous derivatives.

The value of $z_\Delta(\chi,\tau)$ is obtained with the Schwarz formula

$$z_\Delta(\chi,\tau)=\frac{1}{2}\int_{-\infty}^{\infty}y_\Delta(\sigma,\tau)\coth\frac{\pi}{2}(\sigma-\chi)\,\mathrm{d}\sigma-\frac{1}{2}\int_{-\infty}^{\infty}y_\Delta(\sigma+\mathrm{i},\tau)\tanh\frac{\pi}{2}(\sigma-\chi)\,\mathrm{d}\sigma. \tag{25}$$

Differentiating the spline presentation of $z_\Delta(\sigma,\tau)$ with respect to σ, we have

$$\frac{\partial z_\Delta}{\partial\chi}(\chi,\tau)=\frac{1}{2}\int_{-\infty}^{\infty}\frac{\partial y_\Delta}{\partial\sigma}(\sigma,\tau)\coth\frac{\pi}{2}(\sigma-\chi)\,\mathrm{d}\sigma-\frac{1}{2}\int_{-\infty}^{\infty}\frac{\partial y_\Delta}{\partial\sigma}(\sigma+\mathrm{i},\tau)\tanh\frac{\pi}{2}(\sigma-\chi)\,\mathrm{d}\sigma. \tag{26}$$

By using (20), (23) and (24), we obtain the derivative of $\frac{\partial z_\Delta}{\partial \tau}(\chi, \tau_j)$ as

$$\begin{aligned}\frac{\partial z_\Delta}{\partial \tau}(\chi,\tau_j) = \frac{\mathrm{i}}{2}\frac{\mathrm{d}z}{\mathrm{d}w}(\chi,\tau_j)\left\{\left(\frac{1}{g}-1\right)\int_{-\infty}^{\infty}\frac{\partial y_\Delta}{\partial\sigma}(\sigma,\tau_j)\left|\frac{\mathrm{d}w}{\mathrm{d}z}(\sigma,\tau_j)\right|^2\coth\frac{\pi}{2}(\sigma-\chi)\,\mathrm{d}\sigma - \right.\\ -\left(\frac{1}{g}-1\right)\int_{-\infty}^{\infty}\frac{\partial y_\Delta}{\partial\sigma}(\sigma+\mathrm{i},\tau_j)\left|\frac{\mathrm{d}w}{\mathrm{d}z}(\sigma+\mathrm{i},\tau_j)\right|^2\tanh\frac{\pi}{2}(\sigma-\chi)\,\mathrm{d}\sigma + \\ \left.+\frac{1}{g}\int_{-\infty}^{\infty}\frac{\partial x_\Delta}{\partial\sigma}(\sigma,\tau_j)\left|\frac{\mathrm{d}w}{\mathrm{d}z}(\sigma,\tau_j)\right|^2\coth\frac{\pi}{2}(\sigma-\chi)\,\mathrm{d}\sigma\right\} = \\ = \frac{1}{g(\tau)}\left(\frac{1}{g(\tau)}-1\right)(\chi-\mathrm{i})\frac{\mathrm{d}z_\Delta}{\mathrm{d}w}(\chi,\tau_j)+\left(\frac{1}{g(\tau)}-1\right)\frac{1}{2g(\tau)}\frac{\mathrm{d}z}{\mathrm{d}w}(\chi,\tau_j)\times \\ \times\int_{-\infty}^{\infty}\left|\frac{\mathrm{d}z_\Delta}{\mathrm{d}w}(\sigma,\tau_j)\right|^2\left|\frac{\mathrm{d}w}{\mathrm{d}z}(\sigma,\tau_j)\right|^2\coth\frac{\pi}{2}(\sigma-\chi)\,\mathrm{d}\sigma + \\ +\left(\frac{2}{g(\tau)}-1\right)\frac{1}{2}\frac{\mathrm{d}z}{\mathrm{d}w}(\chi,\tau_j)\int_{-\infty}^{\infty}\frac{\partial x_\Delta}{\partial\psi}(\sigma,\tau_j)\left|\frac{\mathrm{d}w}{\mathrm{d}z}(\sigma,\tau_j)\right|^2\coth\frac{\pi}{2}(\sigma-\chi)\,\mathrm{d}\sigma. \end{aligned} \tag{27}$$

The second expression of the derivative $\frac{\partial z_\Delta}{\partial \tau}(\chi, \tau_j)$ is preferable, if the ET shape has singularities, because it does not require integration along the ET boundary.

Now the time step, using an improved Euler method of 2nd order, can be carried out and the process is repeated.

4.3. Testing

The evolution in time of the WT shapes for ET shapes as given by (9) are depicted in Figure 9. Because of symmetry, we present only the right half of each curve.

The convergence to stationary analytic solutions is demonstrated in all cases considered. It should be noted that the sharp ET shape existing for $\gamma = 0{\cdot}5, \alpha = 0{\cdot}9$ can be subjected to numerical calculation as well, owing to the properties of Equation (27).

4.4. Solutions for various ET shapes and gaps

Results of investigations of the machining of a WP featuring a trapezoidal hollow by a plane electrode tool are shown in Figures 10, 11. In Figure 10 the ET moves vertically downwards with dimensionless velocity equal to 1. In Figure 11 the ET does not move. The process is presented in an electrode-tool coordinate system as shown in Figures 10a, 11a and in a WP coordinate system in Figures 10b, 11b. In both cases a flat WP surface is formed asymptotically, but when ET is moving, the gap size becomes stationary; in another case it increases (the process tends to a self-similar behaviour). One can see that, in the first case, a flat surface is forming more rapidly.

The more interesting feature of these examples is the formation initially of self-similar processes in the vicinity of angle points of the dissolving surface. Such solutions can be obtained

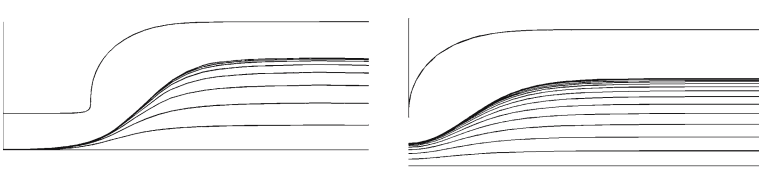

Figure 9. Non-stationary solutions.

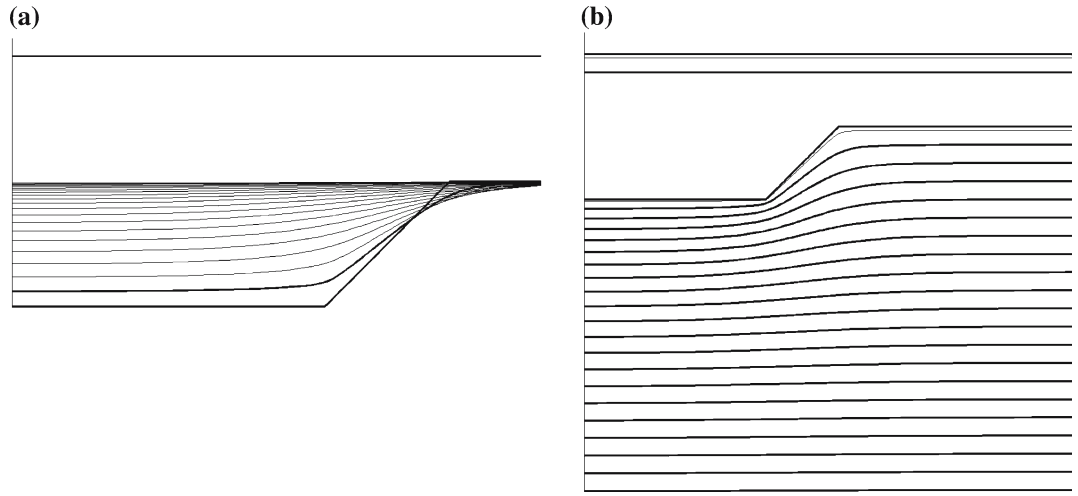

Figure 10. Surface shapes, obtained under plane electrode-tool machining. Electrode tool moves vertically downwards (a) ET coordinate system, $\Delta\tau = 0{\cdot}125$ (b) Work piece coordinate system, $\Delta\tau = 0{\cdot}25$.

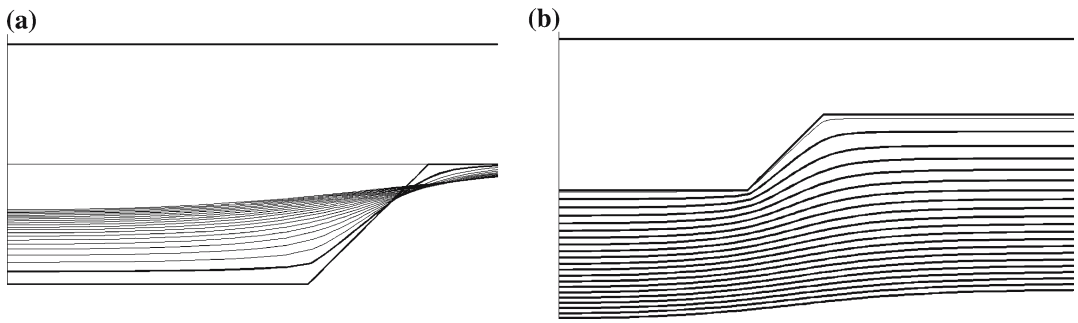

Figure 11. Surface shapes, obtained under unmovable plane electrode tool machining. (a) ET coordinate system, $\Delta\tau = 0{\cdot}125$ (b) Work piece coordinate system, $\Delta\tau = 0{\cdot}25$.

in the same manner as in Section 3.2 (if we consider a two-sided isolated wedge with exterior angle $\delta = 1$ [24]).

The machining by an ET with trapezoidal jut and hollow are illustrated in Figures 12, 13, with a curvilinear jut (see Figure 14). One can see the partial stationary-process rise in the immediate vicinity of the ET zone. Before the general stationary process is established on the whole surface, local stationary configurations are revealed along some parts of the surface. The greater the height of the hollow or jut d, the easier this temporary configuration can be observed. The local stationary shape can be described by the method presented in Section 3.1 with $z(\chi) = e^{\alpha\pi\chi} + (1 + i\tan\alpha\pi)\chi$, where α is the angle between the ET side and the X-axis.

The accuracy of the obtained results was estimated. The demonstrated algorithm allows varying the number of grid nodes and time-step value over a wide range. The accuracy is estimated by the Runge rule. Besides, we may also redistribute the grid nodes on the electrodes during the changing of the inter-electrode shape. Since the electrode-tool shape must remain unchanged in time, the difference of this shape from the initial one may be used as an error estimate. In the results presented here the error was found to be less than 0·1% for 100 nodes.

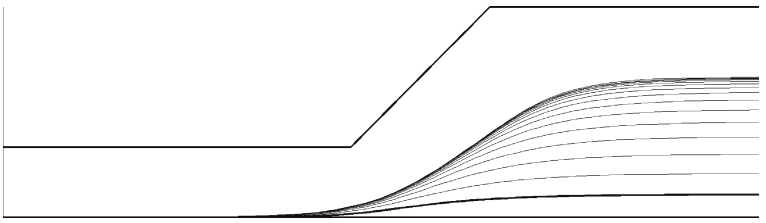

Figure 12. Surface shapes, obtained under machining by an electrode tool with a trapezoidal jut. The electrode tool moves vertically downwards, $\Delta\tau = 0{\cdot}25, d = 2$.

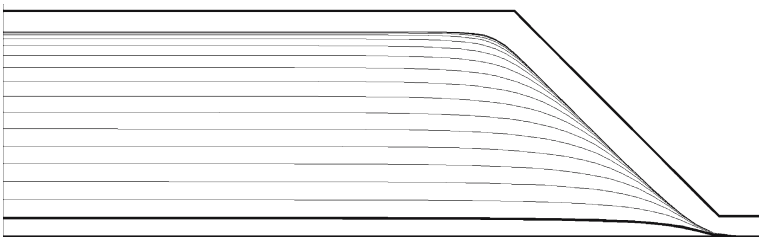

Figure 13. Surface shapes, obtained under machining by ET with a trapezoidal hollow. The ET moves vertically downwards, $\Delta\tau = 1, d = 10$.

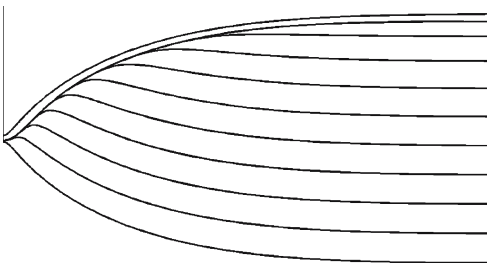

Figure 14. Surface shapes, obtained under machining of a curvilinear work piece surface by a curvilinear electrode tool. The electrode tool moves vertically downwards, $\Delta\tau = 5, d = 20$.

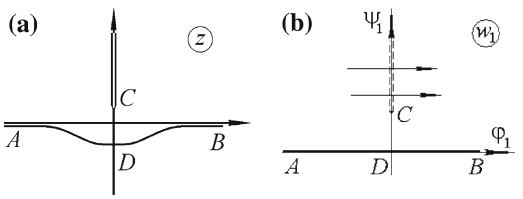

Figure 15. Interelectrode space (a) the physical plane (b) the complex potential of the auxiliary flow.

4.5. Non-stationary machining by a vertical plane electrode tool

The interelectrode space section is shown in Figure 15a, where ADB is a solute metal boundary; C is the position of the edge of the plane ET position vertically. The regions corresponding to the interelectrode space in the complex potential (Figure 1b) and the physical planes are conformally mapped onto a strip χ of width 1/2.

The solution scheme is analogous to that described above. First, it is necessary to find the conformal mapping $z(\chi, 0)$ of the strip $\chi = \sigma + i\upsilon$ onto the initial physical domain z according to the primary interelectrode shape. For the primary plane surface, the mapping has the form

$$z(\chi,0)=g(0)\sinh\pi\chi=g(0)\,z_0(\chi)\,, \tag{28}$$

where g>0.

The $z(\chi,\tau)$ function is written as the sum $z(\chi,\tau)=g(\tau)\,z_0(\chi)+z_\Delta(\chi,\tau)$, so that $\Im\mathrm{m}\,z_\Delta(\sigma+i\upsilon,\tau)\to 0$ when $\sigma\to\pm\infty$. If at the initial time the position of the electrode point is $z_C=0+iy_C$, then $g(0)z_0(\mathrm{i}/2)=z_C$ and $g(0)=y_C$.

On the straight line $\chi=\sigma+\mathrm{i}/2, \Re\mathrm{e}\,z_\Delta(\sigma+\mathrm{i}/2,\tau)=0$, so function $z(\chi,\tau)$ can be analytically extended onto a strip of with 1 (Figure 8). Then on the upper boundary $\chi=\sigma+$ i $\Im\mathrm{m}\,z_\Delta(\sigma+\mathrm{i},\tau)=\Im\mathrm{m}\,z_\Delta(\sigma,\tau)$. Thus, we can use the Schwarz integrals (25), (26) to determine the function $z_\Delta(\chi,\tau)$ and its derivative $\partial z_\Delta/\partial\chi$.

In this problem the boundary condition (5) takes the form

$$\begin{aligned}
&\Im\mathrm{m}\left[\frac{\partial z_\Delta}{\partial\tau}\overline{\frac{\partial z}{\partial\sigma}}\right]=-\frac{\partial\psi}{\partial\sigma}+\frac{\mathrm{d}g}{\mathrm{d}\tau}\frac{\partial y_\Delta}{\partial\sigma}x_0, \qquad \chi=\sigma,\\
&\Im\mathrm{m}\left(\frac{\partial z_\Delta}{\partial\tau}\overline{\frac{\partial z}{\partial\sigma}}\right)=0, \qquad\qquad\qquad\qquad \chi=\sigma+\frac{\mathrm{i}}{2}.
\end{aligned} \tag{29}$$

Since function $\frac{\mathrm{d}w}{\mathrm{d}z}$ has a singularity at the point C $(\chi=\mathrm{i}/2)$, let us consider the complex potential of the auxiliary hydrodynamic problem. Suppose fluid moves with a horizontal velocity at infinity equal to 1, along the lower boundary of the IES penetrating across the ET (see Figure 15b). We have

$$w_1(\chi)=z_0(\chi)=\sinh\pi\chi.$$

The solution can be presented in the form

$$\frac{\partial z_\Delta}{\partial\tau}=\frac{\mathrm{d}z}{\mathrm{d}w_1}f(\chi)=\begin{cases}\dfrac{\partial z}{\partial\varphi_1}f(\chi), & \chi=\sigma,\\ -\mathrm{i}\dfrac{\partial z}{\partial\psi_1}f(\chi), & \chi=\sigma+\dfrac{\mathrm{i}}{2}.\end{cases} \tag{30}$$

Accordingly,

$$\frac{\partial z_\Delta}{\partial\tau}\overline{\frac{\partial z}{\partial\sigma}}=\begin{cases}\left|\dfrac{\mathrm{d}z}{\mathrm{d}w_1}\right|^2\dfrac{\partial\varphi_1}{\partial\sigma}f(\chi), & \chi=\sigma,\\ -\mathrm{i}\left|\dfrac{\mathrm{d}z}{\mathrm{d}w_1}\right|^2\dfrac{\partial\psi_1}{\partial\sigma}f(\chi), & \chi=\sigma+\dfrac{\mathrm{i}}{2}.\end{cases}$$

So, the boundary conditions (29) give

$$\begin{aligned}
&\Im\mathrm{m}\,f(\chi)=\left|\frac{\mathrm{d}w_1}{\mathrm{d}z}\right|^2\left(\frac{\partial\varphi_1}{\partial\sigma}\right)^{-1}\left(\frac{\mathrm{d}g}{\mathrm{d}\tau}\frac{\partial y_\Delta}{\partial\sigma}x_0-\frac{\partial\psi}{\partial\sigma}\right), \qquad \chi=\sigma,\\
&\Re\mathrm{e}\,f(\chi)=0, \qquad \chi=\sigma+\mathrm{i}/2.
\end{aligned} \tag{31}$$

Hence function $f(\chi)$ can be extended analytically onto a strip of width 1 and we can use Schwarz's formula (25) for its determination

$$\frac{\partial z_\Delta}{\partial \tau} = \sinh \pi\chi \frac{\mathrm{d}z}{\mathrm{d}w_1} \left\{ \int_0^\infty \left| \frac{\mathrm{d}w_1}{\mathrm{d}z} \right|^2 \left(\frac{\partial \varphi_1}{\partial \sigma} \right)^{-1} \left(\frac{\mathrm{d}g}{\mathrm{d}\tau} \frac{\partial y_\Delta}{\partial \sigma} x_0 - \frac{\partial \psi}{\partial \sigma} \right) \frac{\mathrm{d}\sigma}{\cosh \pi\sigma - \cosh \pi\chi} + \right.$$

$$\left. + \int_0^\infty \left| \frac{\mathrm{d}w_1}{\mathrm{d}z} \right|^2 \left(\frac{\partial \varphi_1}{\partial \sigma} \right)^{-1} \left(\frac{\mathrm{d}g}{\mathrm{d}\tau} \frac{\partial y_\Delta}{\partial \sigma} x_0 - \frac{\partial \psi}{\partial \sigma} \right) \frac{\mathrm{d}\sigma}{\cosh \pi\sigma + \cosh \pi\chi} \right\} =$$

$$= \frac{1}{g} \frac{\mathrm{d}g}{\mathrm{d}\tau} \frac{\mathrm{d}z_\Delta}{\mathrm{d}w_1} z_0 - 2 \sinh \pi\chi \frac{\mathrm{d}z}{\mathrm{d}w_1} \int_0^\infty \left| \frac{\mathrm{d}w_1}{\mathrm{d}z} \right|^2 \left(\frac{\partial \varphi_1}{\partial \sigma} \right)^{-1} \frac{\partial \psi}{\partial \sigma} \frac{\cosh \pi\sigma \mathrm{d}\sigma}{\cosh^2 \pi\sigma - \cosh^2 \pi\chi}. \quad (32)$$

Note that the presentation (32) is unique; it is a consequence of the uniqueness of the solution of the homogeneous Riemann-Hilbert problem.

Expressions (25) and (32) for $\chi = \mathrm{i}/2$ are used to determine $g(\tau)$ and $\mathrm{d}g/\mathrm{d}\tau$ with $z_C = 0 + \mathrm{i}y_C(\tau)$ and $\frac{\mathrm{d}y_C}{\mathrm{d}\tau}(\tau)$ taken into account, that is

$$y_C(\tau) = g(\tau) + y_\Delta\left(\frac{\mathrm{i}}{2}, \tau\right) = g(\tau) + 2\int_0^\infty y_\Delta(\sigma, \tau) \frac{\mathrm{d}\sigma}{\cosh \pi\sigma}, \quad (33)$$

$$\frac{\mathrm{d}y_C}{\mathrm{d}\tau}(\tau) = \frac{\mathrm{d}g}{\mathrm{d}\tau}(\tau) + \frac{\partial y_\Delta}{\partial \tau}\left(\frac{\mathrm{i}}{2}, \tau\right) =$$

$$= \frac{\mathrm{d}g}{\mathrm{d}\tau}(\tau) + 2\frac{\mathrm{d}z}{\mathrm{d}w_1}\left(\frac{\mathrm{i}}{2}, \tau\right) \int_0^\infty \left| \frac{\mathrm{d}w_1}{\mathrm{d}z} \right|^2 \left(\frac{\partial \varphi_1}{\partial \sigma} \right)^{-1} \left(\frac{\mathrm{d}g}{\mathrm{d}\tau} \frac{\partial y_\Delta}{\partial \sigma} x_0 - \frac{\partial \psi}{\partial \sigma} \right) \frac{\mathrm{d}\sigma}{\cosh \pi\sigma}. \quad (34)$$

Numerical results of machining by an immobile ET, the edge of which is at a distance $y_C = 1$ from the initial position of the WP, are shown in Figure 16. In Figure 16b the curves are scaled in such a way that the distance OD is constant. This serves to illustrate that the non-stationary shapes approach the self-similar one (lower curve in Figure 16a and the upper curve in Figure 16b), which is one of the cases mentioned above (Figure 6, $\gamma = 1$). The analytical expression of this self-similar solution is

$$z(\zeta) = \frac{2}{\pi}\left[\sqrt{\zeta - 1} + \frac{1}{\sqrt{\zeta}}\left(\log\left(\sqrt{\zeta} + \sqrt{\zeta - 1}\right) - \mathrm{i}\frac{\pi}{2}\right)\right].$$

One can observe that the self-similar solution approaches the numerical solution very fast.

Shapes of the anodic surface during electrochemical machining with a moving ET are shown in Figure 17. The electrode tool moves with constant speed, equal to 1 (the drawings are rotated about 90°). The initial distance between ET and WP is equal to 1.

In Figure 17a the coordinate system does not move; in Figure 17b the coordinate system is connected with ET, $\Delta\tau = 25$. In Figure 17c a coordinate system and scale factor were chosen such that the convergence of WP to a self-similar form is visible. For this purpose the

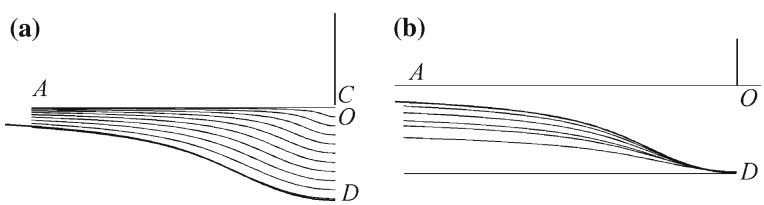

Figure 16. Anodic surface shapes obtained by electrochemical solution with the help of the plane electrode tool for $y_C = 1$: (a) in the usual scale, (b) the scale unit is the OD length.

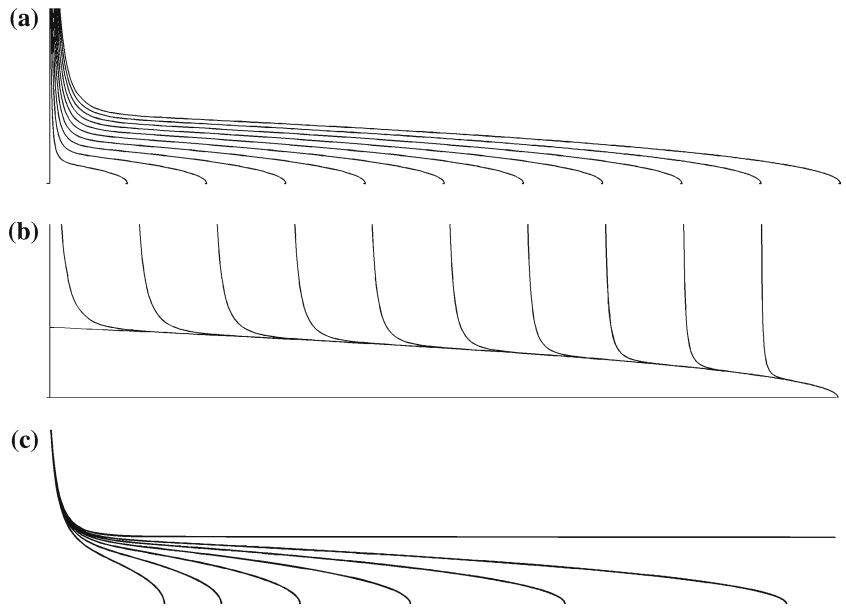

Figure 17. The shapes of the WP surface during electrochemical cutting for a moving plane ET (rotated about 90° counterclockwise).

modulus of the intersection point of the surface and the ray drawn at some small angle to the X-axis was assumed to be equal to 1. The corresponding self-similar shape is shown in Figure 5, (curve $\gamma = 1/2$).

Close to the ET edge, the WP shape practically coincides with the stationary shape (Figure 17b). The stationary WP shape is given by the formula $y = (x^2 - 1)/2$; see [4].

4.6. NON-STATIONARY MACHINING BY A WIRE-SHAPED ELECTRODE TOOL

The interelectrode-space section is shown in Figure 15a, where ADB is the solute-metal boundary, C is the position of the point (wire) electrode tool. The shape of the domain in the complex potential plane w, corresponding to the inter-electrode space, is shown in Figure 3b (rotated about 90° clockwise).

By mapping the strip $\chi = \sigma + i\upsilon$ onto the complex-potential domain, we obtain

$$w = \frac{1}{\pi} \log \frac{1 + ie^{\pi\chi}}{1 - ie^{\pi\chi}}, \quad \frac{dw}{d\chi} = \frac{i}{\cosh \pi\chi}.$$

In all other respects the method described in Section 4.5 is applicable.

The solution of the problem for a stationary ET is shown in Figure 18. The distance between the electrode tool and initial work-piece surface y_C equals 1. Because of symmetry, we present only half of each curve. One can observe the convergence of the WP to a self-similar shape as given by (18) (the lower curve in the Figure 18a and the upper curve in Figure 18b).

In Figure 19 we present results for the dissolution of a curvilinear initial surface which are obtained for a stationary wire-electrode tool, situated at a height $y_C = 0$. These results show the convergence of the process for different initial WP forms dissolving towards a self-similar shape.

Results of machining by an electrode tool moving with constant speed are shown in Figure 20 (the drawings are rotated through 90°). The speed is equal to 1. The electrode tool

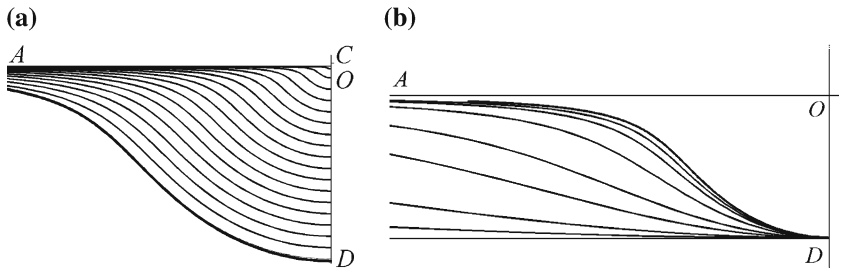

Figure 18. WP surface shapes obtained as a result of electrochemical dissolution by a wire electrode tool for $y_C = 1$: (a) in the usual scale, (b) by the use of OD as the unit length scale.

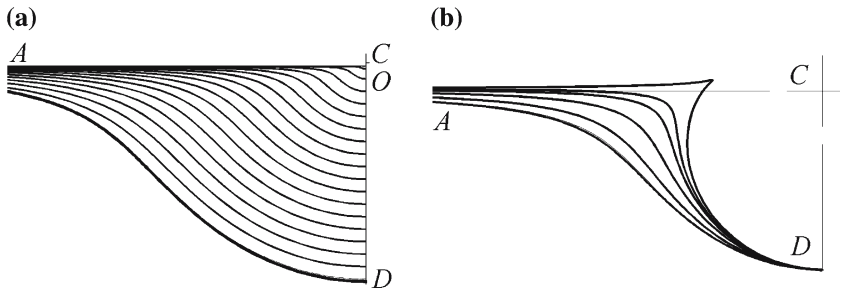

Figure 19. WP surface shapes obtained as a result of electrochemical dissolution by a wire-electrode tool with $y_C = 0$: (a) in the usual scale, (b) the scale unit is CD.

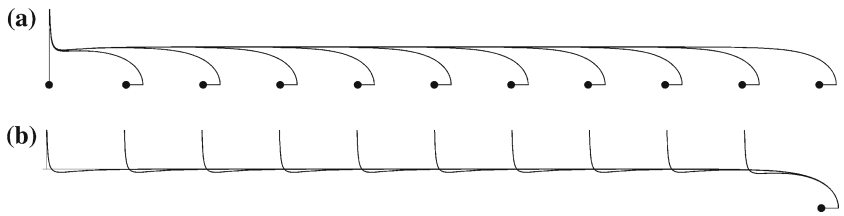

Figure 20. WP surface shapes obtained by a moving electrode tool in a coordinate system which is connected with: (a) initial WP surface, (b) electrode tool.

is denoted as a point. The electrode tool moves perpendicularly to the initial surface, which was plane at the beginning of the process.

The presented results allow calculations of the process starting from a singular configuration, when ET touches the WP surface, $y_C(0) = 0$, in $\tau = 0$. We assume that in the beginning the process is self-similar. This assumption is based on two observations: initially the rate of dissolution is much greater than the ET speed V_{et}; the self-similar shape (18) is an attractor (see Figure 19). Then, using (13), (19) we can find the relation between the dimensionless time and the shift of the lower point of the dissolved surface

$$\Delta_\tau = \frac{1}{2\lambda}\Delta_y^2 = \frac{3\pi}{4}\Delta_y^2,$$

where Δ_τ is the dimensionless time of the self-similar step, Δ_y is the corresponding shift of the lower point of the surface. As ET moves, Δ_τ is the simultaneous ET shift, *i.e.*, the error of the model. However, if $\Delta_y \ll 1$, then $\Delta_\tau \ll \Delta_y$.

It is obvious from Figure 20b that the convergence to a stationary process occurs in the vicinity of the ET. The stationary surface shape is given as ([4])

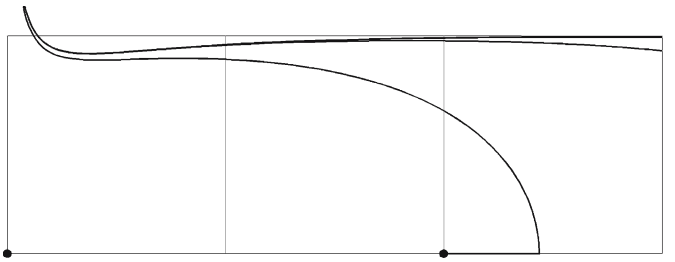

Figure 21. Formation of final WP surface shape.

$$y = -\frac{1}{\pi}\log(2\cos\pi x).$$

Figure 21 shows the formation of the final shape of a WP surface. One can see the narrowing of the slot to the relative value 0·91985, which is explained by the proximity of the starting ET position to the primary WP surface. Calculation shows that this narrowing rapidly disappears when the initial gap $y_C(0)$ increases. The curvature ω of this surface is in the range $-11{\cdot}3 \le \omega \le \pi$.

5. Conclusion

In this paper problems concerning the calculation of nonstationary electrochemical machining have been considered. The effective numerical-analytical method was developed to investigate prolonged transient processes with high accuracy. This method differs from the usual ones by using analytical solutions of the Hele-Shaw problem to obtain the partial time derivative of the work-piece-surface coordinates. It allows raising the accuracy up to order 3 and limit the rate of computational time increase to n^2 (n is the number of nodes). Moreover, it allows control of the node positions, thus increasing the stability of the numerical solution. The choice of the parametrical domain shape (a strip) and removing the singularities of the solution also improve the method.

Exact solutions of some stationary and self-similar problems were obtained independently. The self-similar solutions were obtained by a reduction to an auxiliary hydrodynamical problem. This problem was solved with the help of conformal mapping of circular triangles. The method developed is more straightforward than the usual ones and simplifies the solution process.

The presented examples show that, in the considered processes, the formation of stable configurations close to self-similar or stationary ones takes place sequentially or simultaneously. These configurations are described by the analytical solutions presented in the paper which are related to different variants of the Hele-Shaw problem.

Many other examples may be considered to confirm the assumption that a self-similar solution is an attractor in these cases, when the electrode tool or some part of it does not move towards the work-piece surface. In the case of a moving electrode tool, the stationary solution is such an attractor. The method developed for solving the nonstationary problem gives the opportunity to obtain long-time solutions that retain high accuracy and stability.

We can now formulate the following hypothesis. For a large-enough time every nonstationary electrochemical-machining, ECM process (with ideality assumed) transforms the work-piece surface into a combination of stationary, self-similar and final (as depicted in

Figure 21) sections with transient regions between them. As is obvious from the above, these three forms exhaust the set of asymptotic configurations for an ideal ECM. This concerns not only point, plate-like or wedge-shaped electrode tools. For example, on a large scale, an ET with circular, parabolic or hyperbolic sections looks like a point, a plate and a wedge ET, respectively. The work piece with any limited shape transforms into one or several parts, having circular sections with radii tending to zero. And so on.

A very important question for further investigations is taking account of the electrodes' nonequipotentiality and inconstant current efficiency. Some different limiting cases may occur in these processes. But studying the process with some experimental dependencies gives partial results only. It gives very little information to the researcher, because the actual functions depend on the physical parameters of the real process and can differ essentially. So, for a total study of the problem, it is necessary first to obtain a compact form of inherent dependencies, while using a minimal number of empirical parameters.

The Hele-Shaw problem has many different physical applications. The results obtained can be used for modelling in the fields of hydrodynamics, multiphase flows, etc. Besides, the electrochemical application presents a new problem that is of interest in the theory of Hele-Shaw problems.

References

1. J.A. McGeough, *Principles of Electrochemical Machining.* London: Chapman and Hall (1974) 290 pp.
2. A.D. Davydov and J. Kozak, *High Speed Electrochemical Shaping.* Moscow: Nauka (1990) 290 pp (in Russian).
3. V.P. Zhitnikov and A.N. Zaytsev, *Mathematical Modeling of Electrochemical Machining.* Ufa Techn. Univ. (1996) 221 pp (in Russian).
4. V.V. Klokov, *Electrochemical Shaping.* Kazan Univ. (1984) 80 pp (in Russian).
5. A.H. Karimov, V.V. Klokov and E.I. Filatov, *Methods of Electrochemical Shaping Calculation.* Kazan Univ. (1990) 386 pp (in Russian).
6. G.S. Suvorova, G.R. Engelhart and N.G. Zaydman, One-dimension approximation in electrochemical shaping of engine details. *Electr. Mach. Mat.* 6 (1982) 17–23 (in Russian).
7. P. Novak, I. Rousaz, A. Kimla, *et al.*, Mathematical simulation of electrochemical machining. In: J. Kozak (ed.), *Proc. Int. Sch. ECMM-88*, Lubnevitsy, Poland (1988) pp. 100–115.
8. J. Pandey, Finite element approach to the two dimensional analysis of ECM. *J. Precis. Eng*. 1 (1980) 23–28.
9. S. Christiansen and H. Rasmussen, Numerical solutions for two-dimensional annular electrochemical machining problems. *J. Inst. Math. Appl*. 18 (1976) 295–307.
10. A. West, C. Madore, M. Moltosz and D. Landolt, Shape changes during through-mask electrochemical micromachining of thin metal films. *J. Electrochem. Soc.* 2/139 (1992) 499–506.
11. V.M. Volgin and A. D. Davydov, Modeling of multistage electrochemical shaping. *J. Mat. Proc. Technol.* 149 (2004) 466–471.
12. M. Purcar, L. Bortels, B. Van den Bossche and J. Deconinck, 3D electrochemical machining computer simulations. *J. Mat. Proc. Technol.* 149 (2004) 472–478.
13. H.S. Hele-Shaw, The flow of water. *Nature* 58/1489 (1898) 34–36.
14. H.S. Hele-Shaw, On the motion of a viscous fluid between two parallel plates. *London: Trans. Royal Inst. Nav. Archit*. 40 (1898) 21.
15. S.D. Howison, Complex variable methods in Hele-Shaw moving boundary problems. *Eur. J. Appl. Math*. 3 (1992) 209–224.
16. S.D. Howison, J.R. Ockendon and A.A. Lacey, Singularity development in moving boundary problems. *Q. J. Mech. Appl. Math*. 38 (1985) 343–360.
17. B. Gustafsson and A. Vasil'ev, *Conformal and Potential Analysis in Hele-Shaw Cells*. Stockholm-Valparaiso (2004) 189 pp. www.math.kth.se/∼gbjorn/
18. P. Ya. Polubarinova-Kochina, On a problem of the motion of the contour of a petroleum shell. *Dokl. Akad. Nauk USSR* 47 (1945) 254–257 (in Russian).

19. P. Ya. Polubarinova-Kochina, Concerning unsteady motions in the theory of filtration. *Prikl. Matem. Mech.* 9 (1945) 79–90 (in Russian).
20. P. Ya. Polubarinova-Kochina, *Theory of Groundwater Movement*. Princeton: Princeton University Press (1962) 350 pp.
21. S.D. Howison and J.R. King, Explicit solutions to six free boundary problems in fluid flow and diffusion. *IMA J. Appl. Math*. 42 (1989) 155–175.
22. R.V. Craster, Two related free boundary problems. *IMA J. Appl. Math*. 52 (1994) 253–270.
23. V.P. Zhitnikov, N.M. Sherykhalina and A.R. Urakov, Application of method of singularities isolation for hydrodynamical and electrochemical problems solution. In: A.G. Terentiev (ed.), *Dynamics of Continuous Media With Free Boundaries*. Cheboksary: Chuvash University (1996) pp. 97–106 (in Russian).
24. V.P. Zhitnikov and A.R. Urakov, Self-similar solution of non-stationary problem of electrochemical machining. *Izvestiya VUZov. Mashinostroenie* 1/4–6 (1998) 108–115 (in Russian).
25. G.I. Fedorova and V.P. Zhitnikov, The solution of the problem of self-similar processing by wedge tool electrode with the help of the methods of the complex variable functions theory. In: N. Yussupova (ed.), *Proc. Fifth International Workshop CSIT'2003*, Ufa, Russia (2003) pp. 256–258.
26. V.P. Zhitnikov, A.R. Urakov and A.V. Gutsunaev, Numerico-analitical method for non-stationary ECM problems solution. *Electr. Mach. Mat.* 2/196, (1999) 4–9 (in Russian).
27. V.P. Zhitnikov, G.I. Fedorova, O.V. Zinatullina and A.V. Kamashev, Simulation of non-stationary processes of electrochemical machining. *J. Mat. Proc. Technol.* 149 (2004) 398–403.